amcs

PATH PLANNING FOR AN AUTONOMOUS UNDERWATER VEHICLE IN A CLUTTERED UNDERWATER ENVIRONMENT BASED ON THE HEAT METHOD

KAIYUE SUN [a], XIANGYANG LIU [a,*]

[a]School of Science
Hohai University, Nanjing, Jiangsu, 211100, China
e-mail: `liuxy@hhu.edu.cn`

This paper proposes a novel autonomous underwater vehicle path planning algorithm in a cluttered underwater environment based on the heat method. The algorithm calculates the isotropic and anisotropic geodesic distances by adding the direction and magnitude of the currents to the heat method, which is named the anisotropy-based heat method. Taking account of the relevant influence of the environment on the cost functions, such as currents, obstacles and turn of the vehicle, an efficient collision-free and energy-optimized path solution can be obtained. Simulation results show that the anisotropy-based heat method is able to find a good trajectory in both static and dynamic clutter fields (including uncertain obstacles and changing currents). Compared with the fast marching (FM) algorithm, the anisotropy-based heat method is not only robust, flexible, and simple to implement, but it also greatly saves time consumption and memory footprint in a time-variant environment. Finally, the evaluation criteria of paths are proposed in terms of length, arrival time, energy consumption, and smoothness.

Keywords: autonomous underwater vehicle, path planning, heat method, heat diffusion, cost function.

1. Introduction

Autonomous underwater vehicles (AUVs) are defined as a class of submerged marine robots using various enabling technologies to navigate and perform numerous tasks (Zeng *et al.*, 2015). AUVs have numerous applications including surveillance and reconnaissance, anti-submarine assignment, water profile sampling and littoral ocean floor mapping, etc. Many factors have a great impact on the feasibility and energy requirements of generating an underwater trajectory from the initial to the destination position, such as obstacles, current direction and velocity, time, terrain and performance of AUVs.

The level of autonomy achieved by AUVs is chiefly determined by their performance in pre-generative path planning and re-planning. The problem of pre-generative AUV path planning in anisotropic environments aims to optimize the various aspects of performance comprehensively, such as safety, energy consumption, travel time, etc. Based on these pre-generative algorithms, path replanning for the time-vary ocean environment and underwater terrain-aided navigation combines the terrain

database with terrain contour matching, which improves the accuracy and reliability of the final paths.

Traditionally, path planning for AUVs has been related to safety conditions, and the path should be devoid of known or unknown obstacles or hazardous areas. Artificial potential field algorithms (Cheng *et al.*, 2015) generate safe paths by introducing an artificial potential field around the obstacles preventing vehicles from collision (Hedjar and Bounkhel, 2019). In graph search methods, such as Dijkstra's algorithm (Niu *et al.*, 2018; 2020), the A* algorithm (Koay and Chitre, 2013; Singh *et al.*, 2018) and the D* algorithm, a chart or graph is produced to show free space where no collision will occur, as well as forbidden areas. These methods fast solve low-dimensional problems; however, they are commonly criticized for their discrete state transitions, which unnaturally constrain the motion of a vehicle to the limited direction.

In the quasi-static current field or the time-varying dynamic current field, optimizing the energy cost of traveling in ocean environments is also an important goal in AUV mission planning. Many of the developed planning algorithms integrated the current map with an

---

*Corresponding author

evolutionary path planner (Klaučo *et al.*, 2016; Chen *et al.*, 2018; Makdah *et al.*, 2019), providing an energy efficient path with the limitation of monotonicity in one coordinate of the path. Particle swarm optimization (Witt and Dunbabin, 2008; Mahmoud Zadeh *et al.*, 2017; Wu, 2019) was studied for energy conservation by taking advantage of the time-varying ocean currents, which does not incorporate survival of the fittest and has no conventional evolutionary operators.

In a more common situation, when the thrust power is kept constant during the mission, the optimization of energy consumption agrees with the extraction of the minimum-time path. A fast marching-based (FM) approach was presented by Pêtrès *et al.* (2007) to obtain the minimum time path in a given field, in which only linear cost functions can be used. A novel multi-layered fast marching method (Song *et al.*, 2015; 2017) was proposed for path planning in a time-variant maritime environment, which concerned the surface current and winds. Similar path planners that apply wavefront methods (Soulignac *et al.*, 2008; Soulignac, 2011) and level set methods (Lolla *et al.*, 2012) could obtain the time-optimal paths by using the current fields.

Differing from the FM algorithm based on wave propagation, this paper will use the heat method (Crane *et al.*, 2013; 2017) to calculate the shortest time path, which finds the relationship between geodesic distance and heat by diffusion. The heat method is more suitable for high-dimensional problems, and is not constrained to the need for non-obtuse triangulations or an iterative unfolding procedure. In the following, we present a novel anisotropy-based heat method to solve the AUV path planning problem, while taking into account various factors in the underwater environment, including obstacles, currents, terrain, and energy consumption of the vehicle. Since the algorithm on the surface itself maintains the terrain features well, a three-dimensional path adapted to the underwater environment and matching the terrain can be obtained by detecting the navigation height of the vehicle above the sea floor.

1.1. Paper outline. This paper is organized as follows. Section 2 introduces the underwater environment settings and triangulation reconstruction, as well as the framework of the heat method, including the main idea and discretization of the gradient and Laplacian. Section 3 presents a novel heat method for the AUV path planning problem, which considers the isotropy and anisotropy of geodesic distance. Various factors of the underwater environment are taken into account to obtain a feasible and energy-optimized path solution, including obstacles, current flows, smoothness and terrain. Section 4 shows some simulated experimental results, including paths generated on static and dynamic clutter fields. In addition, we also compare the paths generated by the

anisotropy-based heat method and other algorithms in terms of length, arrival time, energy consumption, and smoothness. Section 5 provides some concluding remarks and possible directions for future work.

2. Environment and the framework

2.1. Underwater environment. AUVs operating very close to the sea floor are increasingly used in the oil and gas market, or in close proximity to offshore industrial structures. They also perform some scientific research tasks, such as deep sea bottom flora and fauna image acquisition. To plan a feasible underwater navigation path, it is required to make full use of sampled data of an ocean simulation. The ocean simulation data samples provide information about the two-dimensional ocean current and sea floor terrains, such as islands, reefs, corals, sand banks.

Graph-based methods traditionally partition the search space in a discrete representation of the environment comprised of edges and nodes. However, the discrete graph representation is extremely limited in finding a continuous path on a continuous domain. Based on the sampled data, we can obtain a continuous path on a manifold discretized by the Delaunay triangulation (Peyré *et al.*, 2010), which is more useful in high-dimensional settings. When S is a finite set of N starting points, one defines a segmentation of the $2D$ manifold Ω into Voronoi cells as

$$\mathcal{V}(S) = \{\mathcal{C}_i\}_{i \in I} \quad \text{and} \quad \Omega = \bigcup_{i \in I} \mathcal{C}_i, \qquad (1)$$

where $I = \{0, \ldots, N-1\}$. It defines a triangle face structure $\mathcal{T}(S)$ by looking at the intersection of three cells

$$\mathcal{T}(S) = \{(i, j, k) \setminus \mathcal{C}_i \cap \mathcal{C}_j \cap \mathcal{C}_k \neq \emptyset\}. \qquad (2)$$

Figure 1(a) is a triangle mesh obtained by Voronoi cells.

It is worth mentioning that the path found is a piecewise linear curve that is linear inside each triangle. The path either follows an edge between two triangles, or

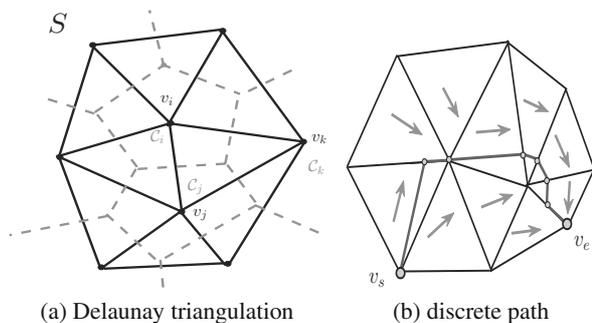(a) Delaunay triangulation   (b) discrete path

Fig. 1. Path on a triangulation.

is parallel to the gradient of the distance function inside a triangle. Figure 1(b) shows an example of discrete geodesic path linking starting point v_s and ending point v_e on a triangle mesh, and the arrow points to the distance gradient direction.

In the ocean environment, in addition to ensuring continuity, an excellent path needs to meet the following criteria:

- avoid and keep a safe distance to obstacles,

- guarantee less travel time at constant speed,

- reduce consumption utilizing a favourable current,

- maintain smoothness and follow terrain features.

Figure 2 is a simulation of a real three-dimensional marine environment, where the black curve is the generated path. The points marked as '×' and '★' represent the start point and the end point, respectively. Since the calculation of the geodesic distance is based on the surface, the generated path can well maintain the characteristics of the seabed terrain.

2.2. Heat framework of the method. The key idea of the heat method is that distance computation can be split into two stages: first computing approximate gradients via heat diffusion, and then using them to recover distance. Rather than obtaining the distance function directly by Varadhan's formula, the method first evaluates a unit vector field that approximates its gradient and then integrates distance by solving a Poisson equation.

The heat method can be applied in any setting where one has a gradient operator (∇), divergence operator ($\nabla \cdot$), and Laplace operator ($\Delta = \nabla \cdot \nabla$). Expressed in terms of those operators, the heat method consists of three basic steps, presented in Algorithm 1.
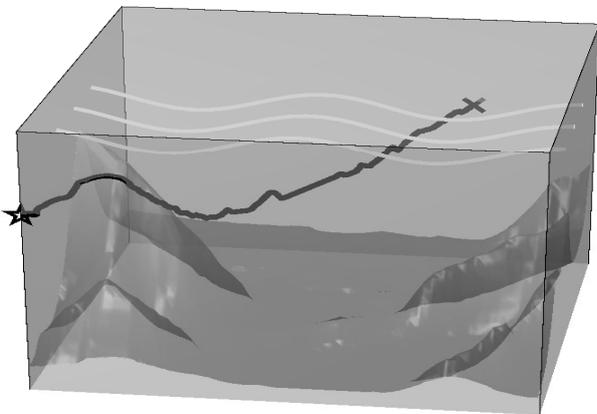

Fig. 2. Simulation of a real 3D marine environment.

Algorithm 1. Heat method.

1: Integrate the heat flow $\dot{u} = \Delta u$ for some fixed time t.
2: Evaluate the vector field $X = -\nabla u_t / |\nabla u_t|$.
3: Solve the Poisson equation $\Delta \phi = \nabla \cdot X$.

As shown in Fig. 3, heat u is allowed to diffuse for a period of time in (a). The temperature gradient ∇u (b) is normalized and negated to get a unit vector field X (c) pointing along the geodesic. A function ϕ whose gradient follows X recovers the final distance in (d). The heat method requires only that the gradient ∇u point in the right direction, that is , parallel to $\nabla \phi$. Since the gradient of the true distance function has unit length (Eikonal equation), the magnitude of u can be safely ignored.

In order to transform a continuous process into a discrete algorithm, the core is to spatially discretize the gradient and Laplacian. Here we only detail the discretization on a triangular mesh, although this method is also applicable to regular grids, point clouds, and polygonal grids (Crane *et al.*, 2013; 2017). A standard discretization of the Laplacian at a vertex i is given by

$$(Lu)_i = \frac{1}{2A_i} \sum_j (\cot \beta_{ij} + \cot \gamma_{ij})(u_j - u_i), \quad (3)$$

where A_i is one third the area of all triangles incident on vertex i, the sum is taken over all neighboring vertices j, and β_{ij}, γ_{ij} are the angles opposing the corresponding edge in Fig. 4(a). The operation can also be expressed via a matrix $L = M^{-1}L_C$, where M is a diagonal matrix containing the vertex areas and L_C is the *cotan operator* representing the remaining sum. The gradient in a given triangle can be expresses succinctly as

$$\nabla u = \frac{1}{2A_f} \sum_i u_i(N \times e_i), \quad (4)$$

where A_f is the area of the triangle, N is its outward unit normal, e_i is the i-th edge vector, and u_i is the value of u at the opposing vertex as in Fig. 4(b). The heat equation and the Poisson equation in Algorithm 1 are discretized on triangular meshes through (3) and (4), so that the geodesic distance calculation can be transformed into solving two sparse linear systems.

We use the A* algorithm, the fast marching algorithm and the heat method to calculate the geodesic distance and backtracking path on the 200×200 surface, respectively (Fig. 5). For a more intuitive and clear comparison, they are presented in two-dimensional graphics, and Fig. 5(a) is a height map of this terrain area. Relative to the graph-based method (A*), the paths on the continuous surface reconstructed by the triangle meshes are not only smoother and continuous, but also avoid steep areas, and maintain the terrain features well.
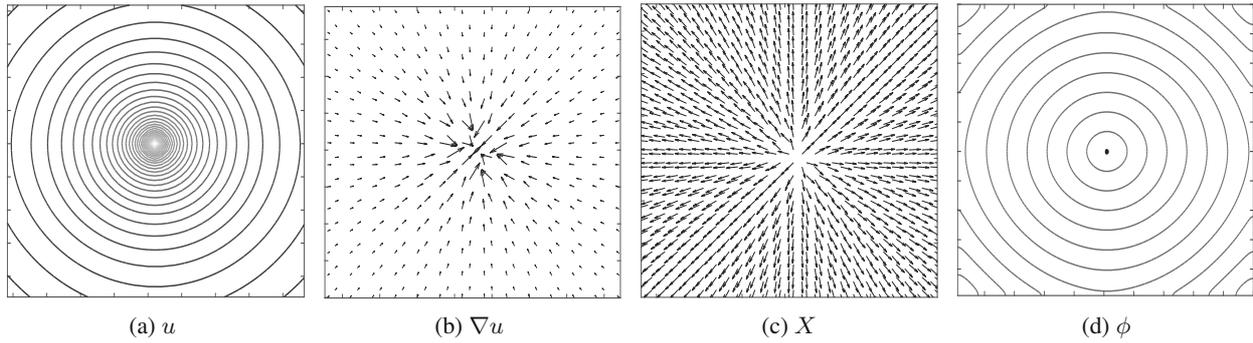
(a) u (b) ∇u (c) X (d) ϕ

Fig. 3. Three steps of the heat method in Algorithm 1.

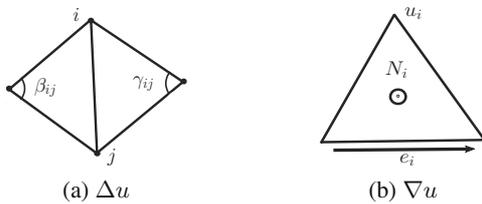(a) Δu (b) ∇u

Fig. 4. Discretization of the Laplacian and gradient in a triangle mesh.

Fast marching is a category of high accuracy algorithms in the state-of-the-art methods for distances. From Figs. 5(c) and (d), we can see that the heat method has a comparable level of accuracy with FM in calculating the geodesic distance, i.e., the minimum arrival time. However, fast marching has an asymptotic complexity of $O(n \log n)$; Crane *et al.* (2017; 2013; 2012) mentioned that since the heat method only involves two sparse linear systems, which can be prefactored once and solved in near-linear time, the amortized cost is thus greatly reduced. Simultaneously, the heat method can avoid the challenges of non-obtuse triangulations or an iterative unfolding procedure, and meshes that are poorly discretized or corrupted by a large amount of noise. In the following, we will apply it more specifically to path planning in an underwater environment.

3. Heat method-based path planning

FM provides numerical algorithms for solving the non-liner equation on triangulated surfaces, while the heat method explores the relationship between heat kernel computation and distances on surfaces. Although these two algorithms are based on different physical models for wave propagation and heat diffusion, they both start from the Eikonal equation.

3.1. Eikonal equation.
The Eikonal equation

$$\|\nabla \phi\| = \tau \tag{5}$$

is subject to the boundary condition $\phi|_\gamma = 0$ over some subset γ of the domain (like a point or a curve). The partial differential equation (5) is nonlinear hyperbolic. In interface evolution problems, the physical meaning of the solution is the shortest time it takes from the curve to reach each point in the computational domain at a speed of $1/\tau$. Intuitively, given a source point, the distance function ϕ must change at a rate of $1/\tau$ (Pêtrès *et al.*, 2007).

In the problem of underwater path planning, τ is a cost function containing a set of internal and external constraints (time, obstacles, currents or fuel consumption). Given a configuration space Ω, which is the set of all possible configuration vertices or faces, containing all static obstacles and all regions free of static obstacles, the cost function τ can be isotropic or anisotropic:

- Isotropic case: the cost function τ depends only on the face x,

$$\tau : \Omega \to \mathbb{R}_+, \quad x \mapsto \tau(x), \quad \tau(x) > 0.$$

- Anisotropic case: τ depends on the face x and a vector $\vec{F}$ of a field of force $\mathcal{F}$,

$$\tau : \Omega \times \mathcal{F} \to \mathbb{R}_+, \quad (x, \vec{F}) \mapsto \tau(x, \vec{F}), \quad \tau(x, \vec{F}) > 0.$$

In AUV path planning, $\mathcal{F}$ is the current force, and each configuration face is assigned a 2D vector $\vec{F}$, which contains the velocity and direction of the current. Note that the heat method uses rules based on the face to calculate gradient variables and other auxiliary variables, which are three-dimensional vectors on the surface.

3.2. Isotropic and anisotropic geodesic distance.
From the heat equation $\dot{u} = \Delta u$, the heat method derives a vector field $-\nabla u$ to approximate the gradient of the geodesic distance $\nabla \phi$. The magnitude can be safely ignored since it is assumed in this method that the gradient of the true distance function has unit length.
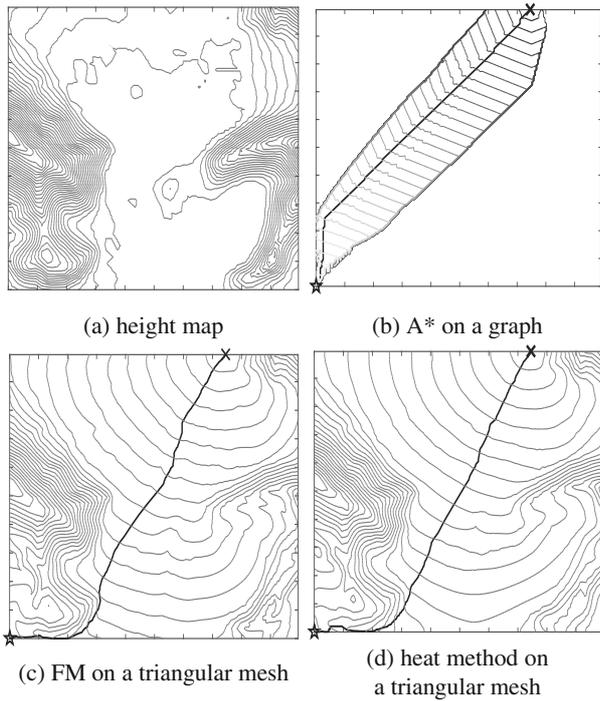
(a) height map

(b) A* on a graph

(c) FM on a triangular mesh

(d) heat method on a triangular mesh

Fig. 5. Examples of distance maps and paths computed over a 200×200 surface (Fig. 2) reconstructed on a graph or triangle mesh.

(a) $\theta_1, \theta_2, \theta_3$

(b) $\widetilde{F}$

(c) X

(d) $\widetilde{X}$

Fig. 6. Effects of different degrees of external forces on the gradient direction of the geodesic distance.

Utilizing a unit vector field to find the closest scalar potential ϕ by solving the Euler–Lagrange equation $\Delta \phi = \nabla \cdot X$, we can only obtain geodesic distances on the Riemannian manifold in the identity metric. However, in most practical applications, such as AUV path planning, computer vision and graphics, it is more necessary to calculate the distance considering cost or in the weighted metric. Following this approach, we use a vector field B containing magnitude and direction to characterize the isotropy and anisotropy of the geodesic distance. Instead of directly normalizing the gradient field, the vector field B is synthesized by adding the scalar cost (weighted metric) and the external force vector to the gradient field.

- Isotropic case: the vector field B is defined by the product of the cost and the unit gradient vector field,

$$B_j = \tau_j \cdot X_j. \tag{6}$$

- Anisotropic case: B is defined by the product of the cost and the synthetic unit vector field,

$$B_j = \tau_j \cdot \widetilde{X}_j, \qquad \widetilde{X} = \frac{-\nabla u + \varepsilon \cdot \vec{F}}{|-\nabla u + \varepsilon \cdot \vec{F}|}. \tag{7}$$

Here, τ_j is a scalar weight (cost) of triangle j, X_j is a unit vector calculated by Step II of the heat method. In the case of anisotr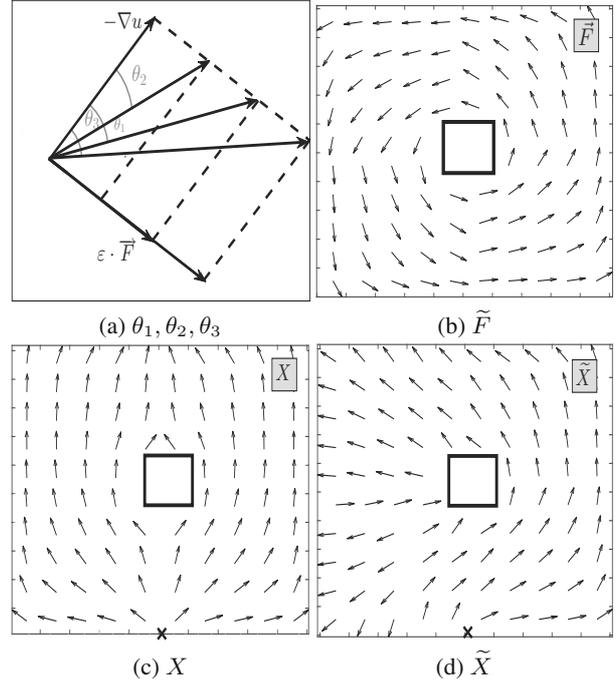opy, the gradient direction $\widetilde{X}$ of the geodesic distance is synthesized by the external force $\vec{F}$ and the opposite direction of heat diffusion $-\nabla u$. Also ε is a control parameter that determines the effect of the external force on the main direction of the distance increment. In Fig. 6(a), $\theta_1, \theta_2, \theta_3$ represent the deviation angle of the synthesized vector from the original gradient direction of heat diffusion, which can indicate the strength of the effect of external force. As the control parameter ε increases, the gradient direction of the geodesic distance deviates further from the direction of heat diffusion, obviously, $\theta_2 < \theta_1 < \theta_3$. Figure 6(b) is a vortex-like current field, and (c), (d) are isotropic and anisotropic unit gradient fields.

The vector field B is defined, and the geodesic distance can be recovered by solving the Poisson equation

$$\Delta \phi = \nabla \cdot B. \tag{8}$$

Based on the discretization of the Laplacian and gradient operators on the triangle mesh, if we let $d = \nabla \cdot B$, the Poisson equation is discretized into a linear system,

$$L_C \phi = d, \tag{9}$$

where L_C is the *cotan operator* representing the remaining sum.

In the above idea, the heat equation is mainly used to find the gradient direction of the distance without

considering magnitude. Furthermore, equivalently, the diffusion of heat flow on a non-uniform medium can also characterize the isotropy and anisotropy of the geodesic distance. The non-uniform medium means that different areas on the object have different values of thermal diffusivity, which depend on the material density of the object itself and the external environmental cost. Define diffusivity as

$$\alpha(x) = D(\text{material}, \tau(x)), \tag{10}$$

where $\alpha(x) \geq 0$ and the function D is inversely proportional to the cost τ, that is, the higher the cost on each triangle x, the slower the heat diffusion. Here, the morphology, density and heat conductivity of the material, which depend on the difference in the internal molecular weight, structure and distribution, also generate a great impact on diffusivity.

With thermal diffusivity, the heat equation in Step I of the heat method can be generalized to a more general form (Yang and Cohen, 2016; Yang *et al.*, 2018),

$$\frac{\partial u}{\partial t} = \text{div}(\alpha(x) \cdot \nabla u). \tag{11}$$

By discretization in time using a single backward Euler step for some fixed time t,

$$[id - t \cdot \text{div}(\alpha \cdot \nabla)]u_t = u_0, \tag{12}$$

heat flow can then be computed by solving the symmetric positive-definite system

$$\left[M - t \cdot \sum_{i=1}^{3} {G_N^i}^T (\alpha_M G_N^i) \right] u = \delta_\gamma, \tag{13}$$

where δ_γ is the Kronecker delta (or an indicator function) over γ, M is a diagonal matrix containing the vertex areas, α_M is a matrix containing the thermal diffusivity on each triangle and G_N^i is the gradient operator obtained from the normal. Also, $\sum$ represents the sum of the elements in the matrix. Figure 7 present the geodesic distances calculated by different thermal diffusivities.

3.3. Energy optimal path planning solution.
Path optimization can be a very complex problem depending on whether the path solution space is constrained, as well as the complexity of the environment and the performance of autonomous underwater vehicles. The objectives of the optimization take into account at least the following aspects: travel time, safety and energy consumption. Assuming that the speed of the vehicle is constant, the minimum-time path can be found by the heat method, which is significantly more effective in high-dimensional settings. For safety, the path should avoid the known forbidden zones, such as obstacles or hazardous areas.
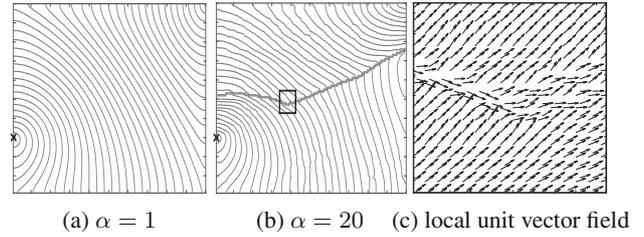

(a) $\alpha = 1$ (b) $\alpha = 20$ (c) local unit vector field

Fig. 7. Geodesic distances with different thermal diffusivity.
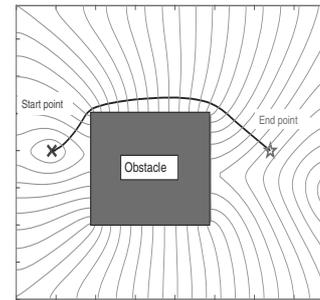

Fig. 8. Path generated by the heat method avoids the obstacle.

Forbidden zone. In the heat method, the calculation of the gradient and Laplace operators is based on faces, whose areas are used repeatedly in the process of solving the heat equation. If we set the thermal diffusivity in (10),

$$\alpha_Z = 0,$$

the heat can be effectively prevented from diffusing on the forbidden zone or obstacles Z, that is, the geodesic distance is ∞, so the path found avoids collision. A similar effect can be obtained by setting the cost function (Fig. 8)

$$\tau_{\text{obst}} = \begin{cases} \infty, & x \in Z, \\ 0, & x \notin Z. \end{cases}$$

Current. How to utilize the current fields in an ocean environment is a key issue of optimizing the energy cost of AUV traveling. The current is highly anisotropic, which not only affects the direction of navigation, but can also greatly reduce energy consumption when used correctly. According to the anisotropic case above, we can use the gradient vector $-\nabla u$ of heat diffusion and the current $\vec{F}$ to synthesize the gradient direction $\widetilde{X}$ of the geodesic distance. However, an apparently traversable path can be unfeasible at certain times when strong currents flow in the opposite direction. In order to make the gradient direction of distance more consistent with the law, and not to depend on the current excessively, we calculate the control parameter in (7),

$$\varepsilon = \mu \cdot \left(\frac{1}{|\mathcal{R}|} \sum_{\mathcal{R}} \frac{|\vec{F}|}{|\nabla u|} \right)^{-1}, \qquad \mu \in (0, 1). \quad (14)$$

Here, the opposite direction refers to $\langle -\nabla u, \vec{F} \rangle < 0$, $\mathcal{R}$ represents the set of all triangles whose angle between $-\nabla u$ and $\vec{F}$ is greater than $90°$, and μ is the influence factor of the current on the final path. Equation (14) shows that, if there are more current directions opposite to heat diffusion directions, the impact of the current on the direction of the geodesic distance will be decreased. Figure 9 shows the effect of the current direction on underwater path planning. Obviously, the path generated by our method (Fig. 9(b)) is more adapted to the behavior of the current.

Energy consumption can be significantly reduced when the current direction is similar to that of navigation (heat diffusion), i.e., $\langle -\nabla u, \vec{F} \rangle \geq 0$. Regardless of the speed of the vehicle, a favourable current can always speed up the vehicle motion, thereby reducing the minimum arrival time. Here we ignore the resistance of the current to the vehicle during travelling in a similar direction, and define the cost of different current speeds by

$$\tau_{\text{speed}} = \frac{2}{1 + \exp(\Upsilon \cdot \omega |\vec{F}|)} \geq 0, \quad (15)$$

where

$$\Upsilon = \begin{cases} 1, & \langle -\nabla u, \vec{F} \rangle \geq 0, \\ -1, & \langle -\nabla u, \vec{F} \rangle < 0 \end{cases}$$

is a signum function, $\Upsilon \cdot |\vec{F}|$ is a directional real number representing the magnitude of the current and ω is a control parameter of the current velocity, which determines the degree of the influence of the current speed on the path. Equation (15) accounts for the resistance and boost effects of the flow velocity on the vehicle from the two perspectives of reversal and the same direction of the water flow. The greater the flow velocity in the reverse direction, the greater the cost; the greater the flow velocity in the same direction, the more energy will be saved. The setting of the cost function can make the planned path avoid the reverse current and maximize the navigation with the assistance of the same current. Also, τ_{speed} can be turned into the isotropic version (6) or the anisotropic version (7) of the heat method and calculate geodesic distances.

Smoothness of turn. Optimizing energy consumption also requires vehicles to avoid large-scale turns and lifts as much as possible. The current opposite to the vehicle will make the synthetic direction deviate greatly from the navigation direction (the direction in which the geodesic distance increases), thereby increasing energy
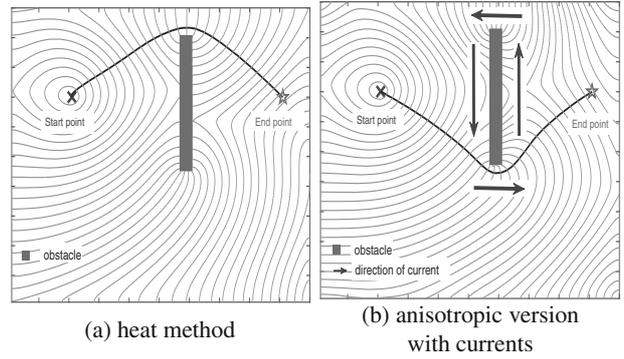

(a) heat method   (b) anisotropic version with currents

Fig. 9. Effect of the current direction on underwater path planning.

(a) heat method with an obstacle   (b) isotropic version with τ_{turn}

(c) $\alpha = 20$ (d) anisotropic version with τ_{turn}
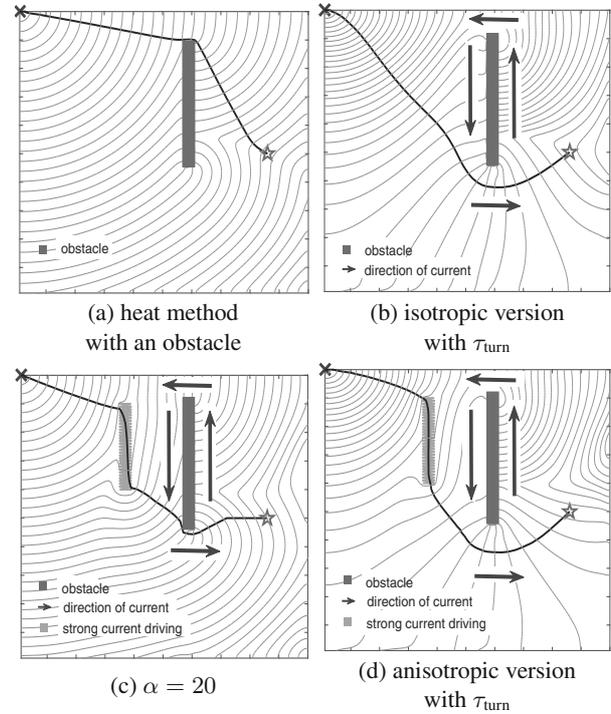
Fig. 10. Effect of the cost of turn on underwater path planning.

consumption. For this, we define the cost of turn,

$$\tau_{\text{turn}} = \kappa \cdot \left(1 - \frac{\langle -\nabla u, \vec{F} \rangle}{|\nabla u| \cdot |\vec{F}|} \right) \geq 0, \quad (16)$$

where κ is a positive gain. It is equivalent to saying that a force favors the vehicle when both are pointing in a similar direction.

Taking into account the cost of turning, the path not only more adapts the behaviour of the current (Fig. 10(b)), but it also becomes smoother and keeps a certain safety distance from the obstacle (Fig. 10(d)). Since the vehicle only needs smooth, rather than acute large-scale turns

during navigation, a lower-performance robot, which has poor hardware equipment and short life, can also perform underwater tasks excellently. Note that the concept can be generalized to path planning in any field of force, like path planning for sailing applications, where $\mathcal{F}$ is a wind field, for instance.

3.4. Algorithm. After calculating the geodesic distance ϕ by the novel heat method, a geodesic curve γ^* (shortest path or minimum time path) between end point v_e and start point v_s can be computed by the gradient descent. This means that γ^* is the numerical solution of the following ordinary differential equation (Cohen and Kimmel, 1997; Peyré *et al.*, 2010):

$$\forall t > 0, \quad \frac{\mathrm{d}\gamma^*(t)}{\mathrm{d}t} = -D^{-1}\nabla\phi, \quad \gamma^*(0) = v_e, \quad (17)$$

where D is a metric tensor in the anisotropic case. For the isotropic case, $D = \alpha^2 I_d$, (17) becomes $\mathrm{d}\gamma^*/\mathrm{d}t = -\nabla\phi$. This technique can be used for any geodesic distance generated by various algorithms, including Dijkstra's method and the fast marching method (Mirebeau, 2014; 2018).

From Section 3.3, in order to obtain an energy-optimized path solution, it is necessary to

---

Algorithm 2. Anisotropy-based heat method.

Require: Triangular mesh (V, F), source vertex v_0, heat diffusion time t, field of force $\mathcal{F}$, thermal diffusivity α, obstacle area Z, parameters ω, κ

Precompute:
1: unit normal field N;
2: triangle area matrix A;
3: vertex areas matrix M;
4: gradient operator G computed by (4);
5: Laplace operator $L = \sum G^{iT}(\alpha G^i)$;

Compute Distance:
  $d : V \to \mathbb{R}$
1: $u \Leftarrow (M + t * L)\backslash\delta$ ▷ Heat diffusion from v_0
    $\delta_{i=v_0} \Leftarrow 1, \delta_{i\neq v_0} \Leftarrow 0$
2: $S \Leftarrow -\nabla u + \varepsilon * \mathcal{F}$ ▷ Synthesis vector field
    $\varepsilon \Leftarrow \text{test}(\mu)$
3: $H \Leftarrow S/|S|$ ▷ Unit vector field
4: $\tau \Leftarrow \tau_{\text{obst}} + \tau_{\text{speed}} + \tau_{\text{turn}}$ ▷ Cost function
    $\tau_{\text{obst}} \Leftarrow \text{obstacle} : Z$
    $\tau_{\text{speed}} \Leftarrow \text{costspeed}(\omega)$
    $\tau_{\text{turn}} \Leftarrow \text{costturn}(\kappa)$
5: $B \Leftarrow \tau \cdot H$ ▷ Gradient vector with cost
6: $d \Leftarrow L\backslash\text{div}(B)$ ▷ Recover geodesic distance

Generate Path:
  Input: Distance map d; Goal vertex v_e; Height Δz
  Output: Final path γ^*
  $\gamma^* \leftarrow$ Eqn. (17)   ▷ Path on surface

---

comprehensively consider various factors such as obstacles, current, smoothness, etc. The total cost function on each triangle face can be expressed as

$$\tau = \tau_{\text{obst}} + \tau_{\text{speed}} + \tau_{\text{turn}}. \quad (18)$$

Algorithm 2 shows the pipeline of the proposed anisotropy-based heat method for AUV path planning, which mainly contains three steps: pre-calculation, distance computation and path generation. The significant benefit of our approach is that it takes into account the isotropy and anisotropy of geodesic distances, and reduces energy consumption in navigation procedures by considering the marine environment. Furthermore, taking advantage of the sea floor terrain information and current makes the generated path more feasible and accurate in a real three-dimensional underwater environment. The heat method itself is more robust and easier to operate, making the algorithm suitable for more complex scenes.

4. Experimental results and a discussion

In this part, we first show the impact of various parameter changes in the algorithm on the final path. Then, the simulation results obtained for the underwater path planning problem through scenarios of different sizes with a static current are shown and analyzed. In the dynamic current field, a path more adapting the behaviour of the current can be re-planned in real time at the rendezvous points. Finally, a comparison of our algorithm with other methods is presented.

4.1. Parameter evaluation. Anisotropic and isotropic heat methods with varying parameters generate different geodesic distance maps and underwater navigation paths. In the following, the results of the path planning for autonomous underwater vehicles using different values of heat diffusivity α in (10), current direction control parameter μ in (14), current flow speed control parameters ω in (15), and turning cost parameter κ in (16) will be presented.

As shown in Fig. 11, the currents in the light grey area represent strong currents with high speed flowing in the direction of the arrow. Here, μ can be used to determine the degree of the effect of the current on the synthesis of the new gradient direction of geodesic distance. As μ continues increasing in Fig. 11, paths generated by the anisotropic version of the heat method avoid more severely adverse current flows, and, simultaneously, the favorable currents are utilized to speed up the vehicle motion. The geodesic distance is larger where the current flow direction significantly deviates from the original heat diffusion direction.

Here, in order to separately show the effect of the cost function on the isotropic version, we set $\mu = 0$. The

parameter ω controlling the current speed continues to rise, increasing the cost gap between navigating upstream and downstream, making the path to make full use of the favorable water flow and reducing consumption. Also, κ can represent the proportion of turning cost to total cost $\tau = \tau_{\text{speed}} + \tau_{\text{turn}}$ in a non-forbidden area, i.e., $\tau_{\text{obst}} = 0$. In order to show the effect of τ_{turn} in the anisotropic version of the heat method, we set $\mu = 0.1$, $\omega = 0.1$. The turning cost can be used not only to calculate the isotropic or anisotropic geodesic distances, but also to ensure that the path is sufficiently smooth. From Fig. 11, the geodesic distance recovered from the unit vector field X or $\widetilde{X}$ in the heat method is uniform, while the contours calculated by using the cost function τ are obviously non-uniform.

4.2. Experimental simulation. To investigate the performance of the proposed isotropic and anisotropic versions of the heat method, the underwater environment is modeled as a three dimensional surface covered by obstacles and ocean currents. In the $N \times M$ operating field, the three-dimensional coordinate values of all points can be used for the Delaunay triangulation. We habitually present a two-dimensional projection map for seeing and comparing the calculated minimum path more clearly, where the dark grey areas and the arrows represent obstacles and water flows, respectively. In the following experiment, all the constant driving speeds are $s = 1$.

Static operating field. Figures 12(a) and (b) present 3D simulated underwater navigation routes in a 100×100 underwater area obtained by the original heat method and our approach taking into account the current field, respectively. Figures 12(c) and (d) show respectively the geodesic distance contour maps calculated by the heat method and the anisotropic version, and the arrows indicate the current field. It is a two-dimensional or three-dimensional vector field, and the average flow velocity is $|\vec{F}| = 1$. The parameter values are set to $\mu = 0.8$, $\omega = 0.5$, and $\kappa = 0.5$. It is apparent that the path generated by our anisotropic algorithm between the starting point ($\times$) and the ending point ($\bigstar$) adapts more the behaviour of the current. This path avoids severely adverse current flows and takes advantage of favourable ones to speed up the vehicle motion and nose dive the energy expenditure.

Dynamic operating field. In a highly uncertain dynamic operating field, the anisotropy-based heat method can still well be used to generate paths based on variable dynamic current fields and real-time updates of detected uncertain obstacles. The key points in the dynamic current field are these rendez-vous points of currents. A key idea for the path planning problem of the dynamic current field can be split into two stages: first find rendez-vous points of currents, and then re-plan the path with our anisotropic
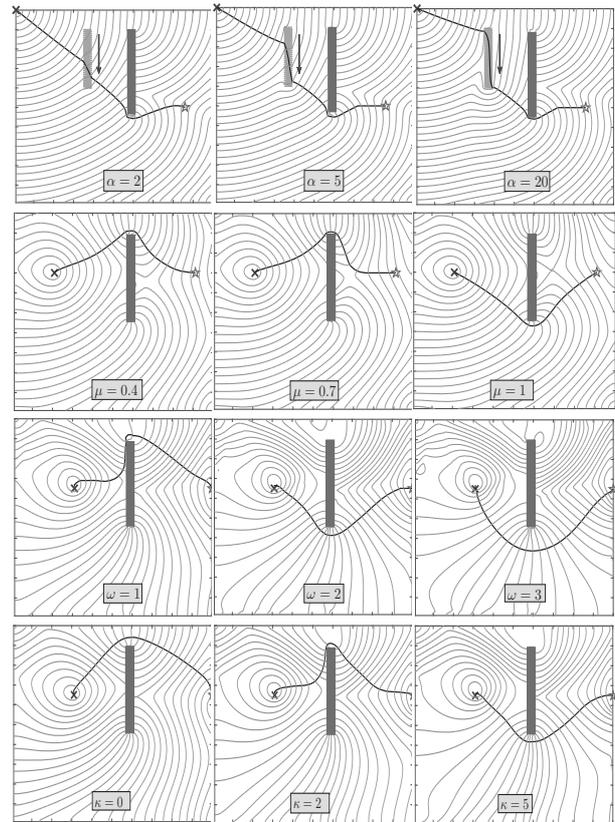

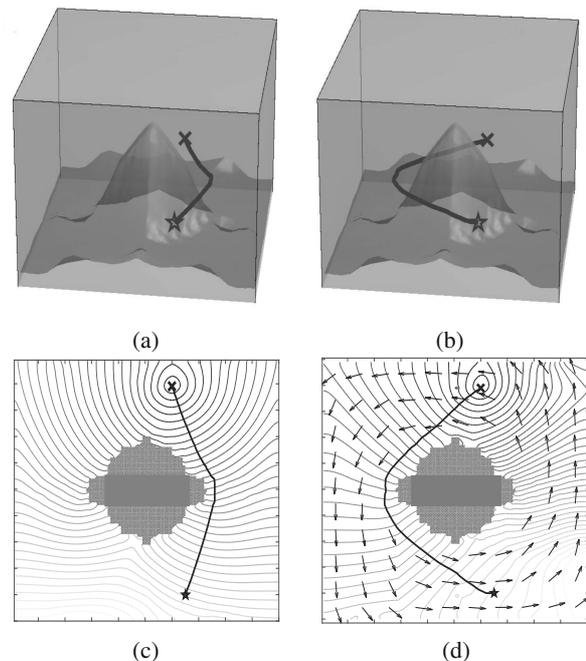Fig. 11. Underwater paths with varying parameters.

Fig. 12. Paths generated in a simulated 100×100 underwater area with or without a current.

heat method. We define all points i that meet the condition

$$\frac{1}{|\mathcal{N}_i|} \sum_{m,n \in \mathcal{N}_i} \frac{\langle \vec{F_m}, \vec{F_n} \rangle}{|\vec{F_m}||\vec{F_n}|} < \rho \qquad (19)$$

as rendez-vous points. Here, $\mathcal{N}_i$ denotes the set of all neighboring faces of vertex i, $\vec{F_m}, \vec{F_n}$ are current flows on triangles m and n, and ρ is the threshold, here set to 0.75. On these rendez-vous points, based on the real-time updated current vector field, we can re-plan a path that utilizes favorable currents to reduce the energy expenditure. The arrows in Figs. 13(a) and (b) indicate the current fields before and after updating, where points in the light grey area are all rendez-vous points of the current field. The average speed of the current is $|\vec{F}| = 1$, and $\mu = 0.5, \omega = 0.5, \kappa = 2$. A complete route is obtained as in Fig. 13(b) by splicing the initial path (thin curve) with the re-planned path (thick curve).

Then, in an operating field with uncertain obstacles, since the gradient descent method used for path backtracking is based on triangular faces to perform iterative operations, a safe and collision-free path can be found successfully by just setting a pass step N_s (number of faces) in real time. The pass step N_s (> 1) can also be set to a small constant, and the smaller the value, the more excellent the result. Assuming that the operating
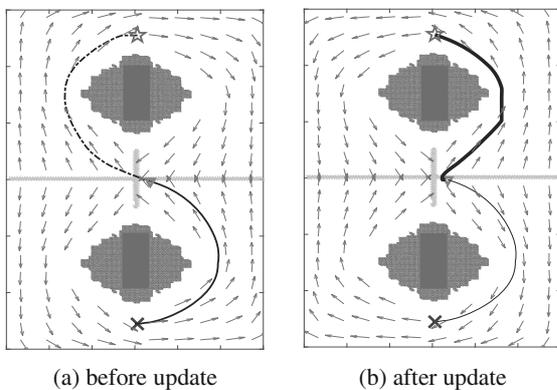

(a) before update   (b) after update

Fig. 13. Path generated in the dynamic current field.

Table 1. Comparison of the execution time of FM and the heat method.

Time [s]	Fast marching		Heat method	
Exaction	Distance	Path	Distance	Path
Initialization	0.26 s	0.87 s	**0.16** s **0.09** s	**0.64** s
First update	0.26 s	0.34 s	**0.11** s	**0.15** s
Second update	0.28 s	0.40 s	**0.11** s	**0.14** s
Third update	0.29 s	0.47 s	**0.13** s	**0.18** s
Fourth update	0.32 s	0.49 s	**0.14** s	**0.18** s
Total time	1.41 s	2.57 s	**0.74** s	**1.29** s

field does not consider the influencing factors of currents in Fig. 14, we updated obstacles four times and calculated the geodesic distance using the heat method to come up with the paths in Figs. 14(a)–(e).

During the four backtracking processes, we set the pass step length to $N_{s_1} = 43, N_{s_2} = 80, N_{s_3} = 45, N_{s_4} = 80$ until we return to the target point. Note that ▼ is the corresponding point after each step. Using the fast marching algorithm to calculate the geodetic distance in real time in the same discrete operating field, and setting the same pass step N_s four times to backtrack and updating the paths, we can get the comparison of the execution times as shown in Table 1. The overall execution time of the algorithm includes the time it takes to calculate the geodesic distance and generate the path. Since a large amount of information (such as the gradient operator) in the pre-calculation of the heat method can be reused, the time can be greatly saved when recalculating the geodesic distance in the continuously updated obstacle field.

4.3. Comparison with others. Figure 15 shows a harbor simulation in which the main exit is obstructed by a net. Naturally, the vehicle must pass through the little back exit to reach the target from the starting point. The simulated current field of the harbor has two different flow directions, the internal current flows clockwise and the external current flows counterclockwise. The whole area consists of 100×100 points, and the dark grey and black areas are walls and nets, respectively.

Figure 16 show the paths generated respectively by the A * algorithm, fast marching, the heat method, and our anisotropic version of the heat method. In the anisotropic experiment, we considered the current field, where the flow velocity $|\vec{F}|$ is different at each point and the average value is 1. The parameters in the cost function are $\mu = 1$, $\omega = 0.1$, $\kappa = 0.1$. The A* algorithm is based on the nodes in the domain, and the latter three methods all calculate the geodesic distance in the same discrete environment constructed by the triangle meshes. Since the A * algorithm is a type of graph search algorithm based on nodes and edges, the path generated by it must be discontinuous. Relative to the fast marching algorithm, the path generated by the heat method can maintain a certain safety distance from obstacles and be smoother. Adding the direction and velocity of the current to the heat method makes the path shown in Fig. 16(d) avoid severely adverse current flows and utilize the favorable ones. In the following, we will evaluate the paths generated from four aspects: length, arrival time, energy consumption and smoothness.

The length of the path can be expressed as the sum of the local Euclidean distances

$$\ell_{\text{total}} = \sum_{j \in f_{\text{path}}} \ell_j, \quad \ell_j = |P_j - P_{j+1}|, \qquad (20)$$

(a) initialization   (b) first update   (c) second update   (d) third update   (e) fourth update
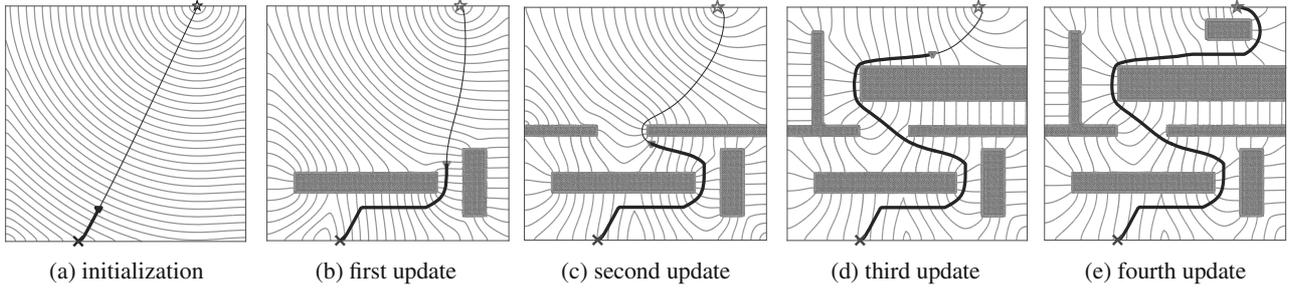
Fig. 14. Real-time path in a cluttered field with updated uncertain/moving obstacles.
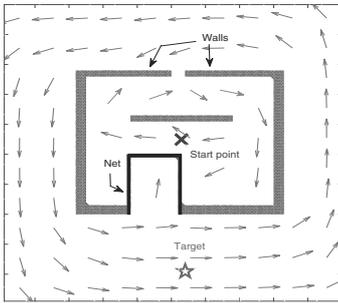
Fig. 15. Simulated current field of a harbor obstructed by a net.

Table 2. Comparison with other methods and an anisotropy-based version.

Algorithm	ℓ_{total}	T_{arrival}	E_{path}	Θ_{mean}
A*	0.7860	1.3005	-	-
Fast marching	**0.4657**	1.1013	3.8003	0.9764
Heat method	0.5015	1.1688	4.0474	0.9942
Aniso-based heat method	0.5428	**0.9221**	**2.8092**	**0.9963**

arrival times, but also consume more energy. The energy consumption of a path can be calculated by

$$E_{\text{path}} = \sum_{j \in f_{\text{path}}} \ell_j \cdot \left(\tau_j^{\text{speed}} + \tau_j^{\text{turn}} \right), \qquad (22)$$

where τ^{speed} and τ^{turn} stand respectively for the cost of the current speed and turn. The product of the local Euclidean distance and the cost of each triangle represents the energy consumption on that face. In addition, we use the cosine of the average turn angle between faces to characterize the smoothness of the path,

$$\Theta_{\text{mean}} = \frac{1}{|f_{\text{path}}|} \sum_{j \in f_{\text{path}}} \frac{\langle V_j, V_{j+1} \rangle}{|V_j||V_{j+1}|}. \qquad (23)$$

Figure 17 shows a path on a triangular mesh, where V_j is the new vector synthesized by the current vector $\vec{F}_j$ and gradient vector $-\nabla u$ obtained by the original heat method, which is used to recover the geodesic distance.

Table 2 presents the comparison results of the four paths in Fig. 16 for the length, arrival time, energy consumption, and smoothness, respectively. When calculating the local Euclidean distance (20) of the paths, in order to adapt to the unitized height value on the terrain, both the x and y coordinates of points are multiplied by a ratio of 0.003. The average speed of the vehicle and the velocity of the current flows are set to $s = 5$ and $|\vec{F}| = 1$, respectively, for calculating the arrival time (21). As shown in Fig. 17, the angle between the gradient vector on the previous V_j and the next triangle V_{j+1} also describes the steering of the vehicle in (22). Since the A*

where f_{path} represents the set of all triangles that the path passes through, while P_j, P_{j+1} are the intersections of the path and the edges of the triangle j, as show below.
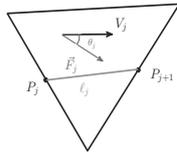
Given the average speed of the vehicle s, the arrival time can be calculated by

$$T_{\text{arrival}} = \sum_{j \in f_{\text{path}}} \frac{\ell_j}{s + \cos \theta_j |\vec{F}_j|}, \qquad (21)$$

$$\cos \theta_j = \frac{\langle V_j, \vec{F}_j \rangle}{|V_j||\vec{F}_j|},$$

with V_j, $\vec{F}_j$ representing the gradient vector and the current on the triangle j. Since the path is backtracked by the gradient descent method according to the geodesic distance, the gradient direction of the point on the path can be regarded as the navigation direction of the vehicle. The current in a similar direction as the gradient speeds up the motion of the vehicle, but it takes more time to sail along the flow of the current in the opposite direction. Severely adverse current flows not only result in longer

(a) A*
(b) fast marching

(c) heat method
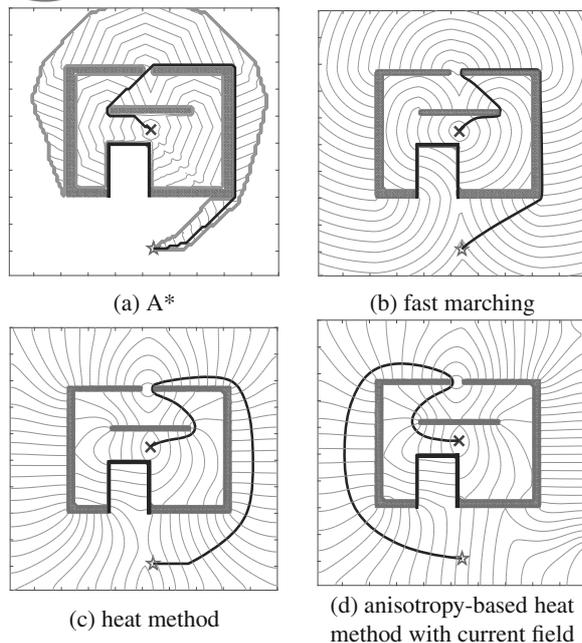(d) anisotropy-based heat method with current field

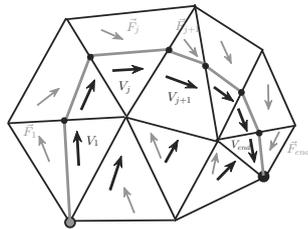Fig. 16. Comparison with other methods for path planning and an anisotropy-based version.

Fig. 17. Path considering current on a triangular mesh.

algorithm is based on discrete nodes and edges, the path obtained has a longer local Euclidean distance and arrival time. Without considering the current flows, although the short length of the path generated by fast marching causes slightly smaller arrival time and energy consumption, the heat method guarantees the safety and smoothness of the path, which is more suitable for 3D space and poor discrete meshes. A large amount of information in the pre-calculation of the heat method can be reused, which can greatly reduce the memory footprint when applied to a dynamic environment. The diffusion time t in the heat method also ensures the flexibility of the algorithm. We set $t = 0.1$ in Figs. 16(c) and (d).

5. Conclusions

The underwater world is a very demanding environment for path planning. This paper proposes a novel non-uniform heat method to calculate an isotropic and anisotropic geodesic distance, and further generate a safe and energy-optimized path in the underwater environment. The path planning algorithm that takes into account the direction of the current and cost function is called the anisotropy-based heat method. Various factors in the underwater environment are used to calculate the cost function, including obstacles, direction and speed of currents, and smoothness of turn. The anisotropy-based heat method is suitable for a wide range of scenarios, such as static current fields, continuously updated dynamic current fields and various uncertain obstacles. Since a good deal of pre-calculated information in the heat method can be reused, path planning on a dynamic current field requires less memory consumption.

Although the heat method and fast marching have similar geodesic distance calculation accuracy, the former is simple to implement and requires only a small execution time. Compared with other similar algorithms, the heat method also can maintain stronger continuity and smoothness of the path. Four indicators for evaluating the AUV path on a triangular mesh are proposed, including length, arrival time, energy consumption and smoothness. The final experimental results show that the anisotropy-based heat method greatly reduces energy consumption of the generated path, and ensures sufficient safety and smoothness.

It is should be mentioned that more complex factors of the underwater environment need to be considered in our future work, including the speed, steering and diving dynamics of the automatic underwater vehicle. Path planning problems in a highly uncertain cluttered field with moving obstacles also need to be solved.

References

Chen, J., Zhu, H., Zhang, L. and Sun, Y. (2018). Research on fuzzy control of path tracking for underwater vehicle based on genetic algorithm optimization, *Ocean Engineering* **156**: 217–223.

Cheng, C., Zhu, D., Bing, S., Chu, Z. and Sheng, Z. (2015). Path planning for autonomous underwater vehicle based on artificial potential field and velocity synthesis, *2015 IEEE 28th Canadian Conference on Electrical and Computer Engineering, Halifax, Canada*, pp. 717–721.

Cohen, L.D. and Kimmel, R. (1997). Global minimum for active contour models: A minimal path approach, *International Journal of Computer Vision* **24**(1): 57–78.

Crane, K., Weischedel, C. and Wardetzky, M. (2012). Geodesics in heat, *Computer Science* **12**(9): 1–10.

Crane, K., Weischedel, C. and Wardetzky, M. (2013). Geodesics in heat: A new approach to computing distance based on heat flow, *ACM Transactions on Graphics* **32**(5): 152.

Crane, K., Weischedel, C. and Wardetzky, M. (2017). The heat method for distance computation, *Communications of the ACM* **60**(11): 90–99.

Hedjar, R. and Bounkhel, M. (2019). An automatic collision avoidance algorithm for multiple marine surface vehicles, *International Journal of Applied Mathematics and Computer Science* **29**(4): 759–768, DOI: 10.2478/amcs-2019-0056.

Klaučo, M., Blažek, S. and Kvasnica, M. (2016). An optimal path planning problem for heterogeneous multi-vehicle systems, *International Journal of Applied Mathematics and Computer Science* **26**(2): 297–308, DOI: 10.1515/amcs-2016-0021.

Koay, T.-B. and Chitre, M. (2013). Energy-efficient path planning for fully propelled AUVs in congested coastal waters, *OCEANS 2013 MTS/IEEE Bergen: The Challenges of the Northern Dimension, Bergen, Norway*, pp. 1–9.

Lolla, T., Ueckermann, M., Yi, K., Haley Jr., K. and Lermusiaux, P. (2012). Path planning in time dependent flow fields using level set methods, *IEEE International Conference on Robotics and Automation, Saint Paul, USA*, pp. 166–173.

MahmoudZadeh, S., Yazdani, A., Sammut, K. and Powers, D. (2017). Online path planning for AUV rendezvous in dynamic cluttered undersea environment using evolutionary algorithms, *Applied Soft Computing* **70**(9): 929–945.

Makdah, A.A.R.A., Daher, N., Asmar, D. and Shammas, E. (2019). Three-dimensional trajectory tracking of a hybrid autonomous underwater vehicle in the presence of underwater current, *Ocean Engineering* **185**: 115–132.

Mirebeau, J.-M. (2014). Anisotropic fast-marching on Cartesian grids using lattice basis reduction, *SIAM Journal on Numerical Analysis* **52**(4): 1573–1599.

Mirebeau, J.-M. (2018). Fast-marching methods for curvature penalized shortest paths, *Journal of Mathematical Imaging and Vision* **60**: 784–815.

Niu, H., Ji, Z., Savvaris, A. and Tsourdos, A. (2020). Energy efficient path planning for unmanned surface vehicle in spatially-temporally variant environment, *Ocean Engineering* **196**: 106766.

Niu, H., Lu, Y., Savvaris, A. and Tsourdos, A. (2018). An energy-efficient path planning algorithm for unmanned surface vehicles, *Ocean Engineering* **161**: 308–321.

Pêtrès, C., Pailhas, Y., Patrón, P., Petillot, Y. and David, L. (2007). Path planning for autonomous underwater vehicles, *IEEE Transactions on Robotics* **23**(2): 331–341.

Peyré, G., Péchaud, M., Keriven, R. and Cohen, L. (2010). Geodesic methods in computer vision and graphics, *Foundations and Trends in Computer Graphics and Vision* **5**(3–4): 197–397.

Singh, Y., Sharma, S., Sutton, R., Hatton, D. and Khan, A. (2018). A constrained A* approach towards optimal path planning for an unmanned surface vehicle in a maritime environment containing dynamic obstacles and ocean currents, *Ocean Engineering* **169**: 187–201.

Song, R., Liu, W., Liu, Y. and Bucknall, R. (2015). A two-layered fast marching path planning algorithm for an unmanned surface vehicle operating in a dynamic environment, *OCEANS 2015, Genova, Italy*, pp. 1–8.

Song, R., Liu, Y. and Bucknall, R. (2017). A multi-layered fast marching method for unmanned surface vehicle path planning in a time-variant maritime environment, *Ocean Engineering* **129**: 301–317.

Soulignac, M. (2011). Feasible and optimal path planning in strong current fields, *IEEE Transactions on Robotics* **27**(1): 89–98.

Soulignac, M., Taillibert, P. and Rueher, M. (2008). Adapting the wavefront expansion in presence of strong currents, *IEEE International Conference on Robotics and Automation, Pasadena, USA,* pp. 1352–1358.

Witt, J. and Dunbabin, M. (2008). Go with the flow: Optimal AUV path planning in coastal environments, *Proceedings of the 2008 Australasian Conference on Robotics and Automation, Sydney, Australia*, pp. 1–9.

Wu, Y. (2019). Coordinated path planning for an unmanned aerial-aquatic vehicle (UAAV) and an autonomous underwater vehicle (AUV) in an underwater target strike mission, *Ocean Engineering* **182**: 162–173.

Yang, F., Chai, L., Chen, D. and Cohen, L. (2018). Geodesic via asymmetric heat diffusion based on Finsler metric, *Asian Conference on Computer Vision, Perth, Australia*, pp. 371–386.

Yang, F. and Cohen, L.D. (2016). Geodesic distance and curves through isotropic and anisotropic heat equations on images and surfaces, *Journal of Mathematical Imaging and Vision* **55**(2): 210–228.

Zeng, Z., Lian, L., Sammut, K., He, F., Tang, Y. and Lammas, A. (2015). A survey on path planning for persistent autonomy of autonomous underwater vehicles, *Ocean Engineering* **110**: 303–313.

Kaiyue Sun is currently a Master's degree student in the Department of Mathematics of Hohai University. Her main research direction is applied mathematics, including computer vision and graphics.

Xiangyang Liu received his PhD in computer software and theory from Shanghai Jiaotong University in 2011. Currently, he is an associate professor and a master tutor of the Department of Information and Computing Science at Hohai University. His main research directions include image and video analysis, data processing, and machine learning.